JOURNAL OF VIROLOGY, July 2011, p. 6390–6402 Vol. 85, No. 13
0022-538X/11/$12.00 doi:10.1128/JVI.00514-11

Multimerization of Adenovirus Serotype 3 Fiber Knob Domains Is Required for Efficient Binding of Virus to Desmoglein 2 and Subsequent Opening of Epithelial Junctions▽

Hongjie Wang,[1,3] ZongYi Li,[1] Roma Yumul,[1] Stephanie Lara,[2] Akseli Hemminki,[3] Pascal Fender,[4] and André Lieber[1,2]*

University of Washington, Division of Medical Genetics, Box 357720, Seattle, Washington 98195[1]; University of Washington, Department of Pathology, Seattle, Washington[2]; Cancer Gene Therapy Group, University of Helsinki & Helsinki University Central Hospital, Helsinki, Finland[3]; and Unit of Virus Host Cell Interactions, UMI3265, CNRS/EMBL/UJF, Grenoble, France[4]

Received 14 March 2011/Accepted 19 April 2011

Recently, we identified desmoglein 2 (DSG2) as the main receptor for a group of species B adenoviruses (Ads), including Ad3, a serotype that is widely distributed in the human population (H. Wang et al., Nat. Med. 17:96–104, 2011). In this study, we have attempted to delineate structural details of the Ad3 interaction with DSG2. For CAR- and CD46-interacting Ad serotypes, attachment to cells can be completely blocked by an excess of recombinant fiber knob protein, while soluble Ad3 fiber knob only inefficiently blocks Ad3 infection. We found that the DSG2-interacting domain(s) within Ad3 is formed by several fiber knob domains that have to be in the spatial constellation that is present in viral particles. Based on this finding, we generated a small recombinant, self-dimerizing protein containing the Ad3 fiber knob (Ad3-K/S/Kn). Ad3-K/S/Kn bound to DSG2 with high affinity and blocked Ad3 infection. We demonstrated by confocal immunofluorescence and transmission electron microscopy analyses that Ad3-K/S/Kn, through its binding to DSG2, triggered the transient opening of intercellular junctions in epithelial cells. The pretreatment of epithelial cells with Ad3-K/S/Kn resulted in increased access to receptors that are localized in or masked by epithelial junctions, e.g., CAR or Her2/*neu*. Ad3-K/S/Kn treatment released CAR from tight junctions and thus increased the transduction of epithelial cells by a serotype Ad5-based vector. Furthermore, the pretreatment of Her2/*neu*-positive breast cancer cells with Ad3-K/S/Kn increased the killing of cancer cells by the Her2/*neu*-targeting monoclonal antibody trastuzumab (Herceptin). This study widens our understanding of how Ads achieve high avidity to their receptors and the infection of epithelial tissue. The small recombinant protein Ad3-K/S/Kn has practical implications for the therapy of epithelial cancer and gene/drug delivery to normal epithelial tissues.

Human adenoviruses (Ads) have been classified into six species (A to F) currently containing 55 serotypes. Members of all species, except species B, utilize the coxsackie-adenovirus receptor (CAR) as a primary attachment receptor. Species B Ad11, Ad16, Ad21, Ad35, and Ad50 utilize CD46 as a receptor, while species B Ad3, Ad7, and Ad14 use desmoglein 2 (DSG2) (31, 33). These receptors determine the *in vitro* tropism of Ads. *In vivo*, particularly after intravenous injection, other mechanisms, such as binding to blood factors and receptor accessibility in tissues, appear to override the *in vitro* rules of Ad tropism (1).

The protruding fiber is the moiety within the Ad capsid that mediates a high-affinity binding to the primary attachment receptor. Each Ad capsid has 12 fibers linked to penton bases. Each fiber consists of a tail domain that is anchored within the penton base, a shaft domain consisting of repeats of up to 14 amino acids that form β-sheets (with the number of repeats ranging from 6 to 23 in different serotypes), and the C-terminal homotrimeric knob domain. For CAR- and CD46-interacting Ads, the knob domain binds with high affinity to the receptor, and soluble fiber knobs completely block infection.

Most studies of Ad interaction with CAR have been done with Ad5. Crystal structure and mutagenesis studies showed that the main interaction between Ad5 and CAR involves one Ad5 fiber knob monomer and one CAR monomer, implying that one trimeric fiber knob binds to three CAR molecules (13). The dissociation constant (K_D) of Ad5 fiber knob interaction with CAR is 20 to 25 nM (18).

Detailed structural studies of species B Ad interaction with CD46 have been done for Ad35 (34) and Ad11 (21). Differently from Ad5 knob-CAR interaction, one CD46 molecule binds between two Ad35 or Ad11 knob monomers. This creates a rigid complex between the trimeric knob and three CD46 units. Moreover, CD46 has a bent configuration, in that upon interaction with the Ad knob it becomes straightened, thereby allowing additional CD46 and knob domains to interact with each other to give a high-affinity interaction (21). Surface plasmon resonance (SPR) analyses of soluble CD46 and Ad35 knobs showed a K_D of ~15.35 nM. The specifics of Ad35 and Ad11 interaction with CD46 also could explain why CD46-interacting species B Ads are released more slowly from endosomes upon uptake into cells than Ad5 (11).

Recently, we identified desmoglein 2 (DSG2) as the main receptor for a group of species B Ads, including Ad3, a sero-

* Corresponding author. Mailing address: University of Washington, Division of Medical Genetics, Box 357720, Seattle, WA 98195. Phone: (206) 221-3973. Fax: (206) 685-8675. E-mail: lieber00@u.washington.edu.

▽ Published ahead of print on 27 April 2011.

type that is widely distributed in the human population (33). DSG2 is a calcium-binding transmembrane glycoprotein belonging to the cadherin protein family. In epithelial cells, DSG2 is a component of the cell-cell adhesion structure (2). Ad3 virus binds to DSG2 with a nanomolar affinity (31). However, in contrast to CAR- and CD46-binding Ads, trimeric Ad3 fiber knob was unable to completely block Ad3 virus binding, even when very high fiber knob concentrations were used, indicating that other or additional capsid moieties were involved in Ad3 binding (30). The efficient blocking of Ad3 infection was achieved with recombinant Ad3 penton-dodecahedral particles (PtDds) consisting of 12 Ad3 fibers linked to penton bases (20). Ad3 fiber and penton must be physically linked, because the preincubation of cells with Ad3 fiber knobs mixed with penton bases did not block Ad3 binding to the degree seen with PtDds (33). These findings suggest that the DSG2-interacting domain(s) within Ad3 is formed by the fiber or fiber/penton only in the spatial constellation that is present in viral particles, i.e., Ad3 virions or PtDds. SPR studies with recombinant PtDds showed a K_D of 2.5 nM. These studies also demonstrated that Ad3 fiber knob dissociated faster from DSG2 than PtDds do. This again indicates that the high-affinity binding of Ad3 requires an additional DSG2 binding site(s) within the fiber shaft, fiber multimerization, and/or a specific spatial constraint of fiber knobs.

In this study, we have attempted to delineate structural details of Ad3 interaction with DSG2. We report that multimers of (trimeric) Ad3 fiber knobs are required for high-affinity DSG2 binding. This is clearly different from the strategy of CAR- and CD46-interacting Ad serotypes to achieve infection. This specific mode of Ad3-DSG2 interaction is functionally crucial for Ad3, because it allows the opening of epithelial junctions.

MATERIALS AND METHODS

Proteins and antibodies. Recombinant human DSG2 protein was from Leinco Technologies, Inc. (St. Louis, MO). The recombinant Ad3 fibers were produced in *Escherichia coli* with N-terminal 6-His tags using the pQE30 expression vector (Qiagen, Valencia, CA) and purified by nickel-nitrilotriacetic acid agarose chromatography as described elsewhere (34). Recombinant Ad3 penton-dodecahedra (PtDds) were produced in insect cells and purified as described previously (8).

The following antibodies were used for immunofluorescence studies: polyclonal goat anti-DSG2 (R&D Systems, Inc., Minneapolis, MN), mouse monoclonal antibody (MAb) anti-DSG2 (clone 6D8) (Cell Sciences, Canton, MA), rabbit anti-claudin 7 (Abcam, Cambridge, MA), fluorescein isothiocyanate (FITC)-conjugated goat anti-adenovirus (Millipore, Billerica, MA), monoclonal anti-6xHis (MCA1396; Serotec), and rabbit anti-ZO-1 antibody (Cell Signaling Technology Inc., Beverly, MA). Polyclonal rabbit antibodies against purified recombinant Ad3 knobs were produced by PickCell Laboratories B.V. (Amsterdam, The Netherlands). Monoclonal anti-DSG2 antibodies 20G1, 7H9, 13B11, 10D2, and 8E5 (12) were purified from hybridoma culture supernatants.

Recombinant Ad3 fiber knobs. The recombinant Ad3 fiber knobs S/Kn, S2/Kn, S3/Kn, S4/Kn, S5/Kn, and S6/Kn were generated by PCR using Ad3 genomic DNA as a template. The PCR products then were cloned into the *E. coli* expression vector pQE30 as BclI/HindIII or BamHI/HindIII fragments. The following primers were used: S6/Kn-forward, 5′-CTGATGAATTCTTGATCAGGGGTTTTAAGTCTTAAATGTGTTAATCC-3′; S5/Kn-forward, 5′-TTACTGATGAATTCTTGATCAGGCTCCCTCCAACTTAAAGTGGGAAGTGGT-3′; S4/Kn-forward, 5′-TTACTGATGAATTCTGGATCCTTAGAAGAAAACATCAAAGTTAACAC-3′; S3/Kn-forward, 5′-TTACTGATGAATTCTGGATCCCATTCTATAAATTTACCAATAGGAAACGGT-3′; S2/Kn-forward, 5′-TTACTGATGAATTCTGGATCCAACAAACTTTGCAGTAAACTCGGAAATGG-3′; S/Kn-forward, 5′-ACCATCACGGATCCAATTCTATTGCACTGAA-3′; reverse for all constructs, 5′-AGCTAATTAAGCTTAGTCATCTTCTCTAATATAGG-3′. For generating the K- or E-coil-containing Ad3 fiber knobs, the following oligonucleotides were annealed and cloned into pQE30 as BamHI fragments: for pQE30-Kcoil, 5′-ATCAAAGGTAAGCGCTTTAAAGGAGAAAGTTTCAGCACTTAAAGAAAAGGTATCCGCTTTAAAGGAGAAAGTTTCAGCACTTAAAGAAAAAGTGTCCGCTCTGAAAGAAG-3′ and 5′-GATCCTTCTTTCAGAGCGGACACTTTTTCTTTAAGTGCTGAAACTTTCTCCTTTAAAGCGGATACCTTTTCTTTAAGTGCTGAAACTTTCTCCTTTAAAGCGCTTACCTTT-3′; for pQE30-Ecoil, 5′-ATCAGAGGTAAGCGCTTTAGAGAAAGAAGTTTCAGCACTTGAGAAGGAGGTATCCGCTTTAGAGAAAGAAGTTTCAGCACTTGAGAAGGAAGTGTCCGCTCTGGAAAAAG-3′ and 5′-GATCCTTTTTCCAGAGCGGACACTTCCTTCTCAAGTGCTGAAACTTCTTTCTCTAAAGCGGATACCTCCTTCTCAAGTGCTGAAACTTCTTTCTCTAAAGCGCTTACCTCT-3′. To generate Ad3-E/S2/Kn and Ad3-K/S2/Kn, the following primers were used: forward, 5′-ATCTAGGATCCGGTGGCGGTTCTGGCGGTGGCTCCGGTGGCGGTTCTAACAAACTTTGCAGTAAACTCGGAAATGGTCTTACATTTGACT-3′; reverse, 5′-AGCTAATTAAGCTTAGTCATCTTCTCTAATATAGG-3′. The PCR products were cloned into the BamHI/HindIII site of pQE30-Kcoil and pQE30-Ecoil. To generate Ad3-E/S/Kn and Ad3-K/S/Kn, the following primers were used: forward, 5′-TTATTGCTACTGGATCCGGTGGCGGTTCTGGCGGTGGCTCCGGTGGCGGTTCTAATTCTATTGCACTGAAAAATAACAC-3′; reverse, 5′-AGCTAATTAAGCTTAGTCATCTTCTCTAATATAGG-3′. The PCR products were cloned into the BamHI/HindIII site of pQE30-Kcoil and pQE30-Ecoil.

Cell lines. 293 (Microbix, Toronto, Ontario, Canada) and HeLa (American Type Culture Collection [ATCC]) cells were cultured in Dulbecco's modified essential medium (DMEM) supplemented with 10% fetal calf serum (FCS), 2 mmol/liter L-glutamine (Glu), 100 U/ml penicillin, and 100 μg/ml streptomycin (pen-strep). BT474-M1 cells (16) were cultured in DMEM-F12 with 10% FBS, 1% pen-strep, and L-glutamine. Colon cancer T84 cells (ATCC CCL-248) were cultured in a 1:1 mixture of Ham's F12 medium and DMEM, 10% FBS, Glu, and pen-strep. To achieve cell polarization, 1.4×10^5 T84 cells were cultured in 6.5-mm Transwell inserts (0.4-μm pore size) (Costar Transwell Clears) for more than 20 days until transepithelial resistance was stable.

Adenoviruses. Propagation, [*methyl*-^{3}H]thymidine labeling, purification, and determining the titers of Ads were performed as described elsewhere (31). Ad5/35-green fluorescent protein (GFP) and Ad5-GFP are Ad5 vectors containing Ad35 and Ad5 fibers and a cytomegalovirus (CMV)-GFP expression cassette (24). Ad3-GFP is a wild-type Ad3-based vector containing a CMV-GFP expression cassette inserted into the E3 region (33). Ad5/3L-GFP and Ad5/3S-GFP are E1/E3-deleted, Ad5-based vectors containing the same CMV-GFP expression cassette inserted into the E3 region. The construction of chimeric Ad vectors followed the protocol described earlier (23). The primer sequences used to construct the chimeric fiber genes were the following: for Ad5/3L-GFP, SF (5′-GACACGGAAACCGGTCCTCCAACTGTGCCTTTTCTTACTCC-3′), SR (5′-GCAGTTGGCTTCTGGTTTTGGACCTGTCCACAAAGTTAGCTTATCATTATTTTTGTTTCC-3′), KF (5′-GGAAACAAAAATAATGATAAGCTAACTTTGTGGACAGGTCCAAAACCAGAAGCCAACTGC-3′), KR (5′-TGAAAAATAAACACGTTGAAACATAACACAACTAGTTCTTTATTCTTGGGCATTTTAGTCATCTTCTCTAATATAGGAAAAGGTAAATG-3′), R1 (5′-CATTTACCTTTTCCTATATTAGAGAAGATGACTAAAATGCCCAAGAATAAAGAACTAGTTGTGTTATGTTTCAACGTGTTTATTTTTCA-3′), and R2 (5′-ATACTTAGGGTACCAATCGATATGGCCACGTGGGTTCTGTGGTCCC-3′); for Ad5/3S-GFP, SF (5′-ACGGAAACCGGTCCTCCAACTGTGCCTTTTCTTACTCCTCCCTTTGTATCCCCCAATGGGTTTCAAGAGAGTCCCCCTGGGGTTTTAAGTCTTAAATGTG-3′), KR (5′-GAAAAATAAACACGTTGAAACATAACACACTCGAGTCTTTATTCTTGGGCATTTTAGTCATCTTCTCTAATATAGGAAAAGGTAAATG-3′), R1 (5′-CATTTACCTTTTCCTATATTAGAGAAGATGACTAAAATGCCCAAGAATAAAGACTCGAGTGTGTTATGTTTCAACGTGTTTATTTTTC-3′), and R2 (5′-ATACTTAGGGTACCAATCGATATGGCCACGTGGGTTCTGTGGTCCC-3′). An SpeI or XhoI restriction site was introduced after the fiber stop codon for Ad5/3L-GFP or Ad5/3S-GFP, respectively. To generate full-length E1/E3-deleted vector genomes, the corresponding shuttle plasmid containing chimeric fiber genes and the GFP expression cassette were inserted in pAdHM4 by homologous recombination in *E. coli* strain BJ1583. The resulting plasmids pAd5/3L-GFP and pAd5/3S-GFP were analyzed by restriction analysis and sequencing. To produce the corresponding viruses, pAd5/3L-GFP and pAd5/3S-GFP were digested with PacI to release the viral genomes and transfected into 293 cells as described before. Recombinant viruses were propagated in 293 cells and purified by standard methods.

Ad particle (viral particle [VP]) concentrations were determined spectrophotometrically by measuring the optical density at 260 nm (OD_{260}), and the deter-

mination of plaque titers (in PFU) was performed using 293 cells as described elsewhere (24). The VP/PFU ratio was 20:1 for all virus preparations.

Attachment and transduction assays. Adherent cells were detached from culture dishes by incubation with EDTA and were washed with phosphate-buffered saline (PBS). A total of 1.8×10^5 cells/tube were resuspended in 100 μl of ice-cold adhesion buffer containing ^{3}H-labeled Ad at a multiplicity of infection (MOI) of 8,000 VP per cell. After 1 h of incubation at 4°C, cells were pelleted and washed twice with 0.5 ml of ice-cold wash buffer (PBS, 1% FBS). After the last wash, the supernatant was removed and the cell-associated radioactivity was determined with a scintillation counter. The number of viral particles (VP) bound per cell was calculated by using the virion-specific radioactivity and the number of cells. For competition studies, .5 μg of competitor (PtDds, fiber knobs, and antibodies) were allowed to attach for 60 min at 4°C in adhesion buffer, and nonbound competitor was removed by washing cells twice with PBS before cells were resuspended in attachment buffer containing ^{3}H-labeled Ad. For transduction studies, cells were exposed to Ad vectors at the indicated MOIs for 1 h and washed, and GFP expression in 20,000 cells was measured by flow cytometry 18 h later.

Ad5 infection studies. In all transduction studies of HeLa, we have used conditions (MOI, virus concentration, and exposure time) that have been optimized previously to be within the linear range of transduction (33).

Western blotting. Mini-Protean precast gels (Bio-Rad, Hercules, CA) with 4 to 15% gradient polyacrylamide were used. For the studies shown in Fig. 2B, a total of 0.5 μg protein was mixed with 2× loading buffer (10 mM Tris-HCl, pH 6.8, 200 mM dithiothreitol [DTT], 4% SDS, 20% glycerol, 0.2% bromophenol blue). Samples either were boiled (B) for 5 min or loaded unboiled (UB). The following running buffer was used: 25 mM Tris, 0.192 M glycine, 0.1% SDS, pH 8.3. After electrophoresis, proteins were transferred to nitrocellulose and incubated with anti-DSG2 antibodies or anti-Ad3 knob antibodies as described previously (33).

Native polyacrylamide gel electrophoresis. For the study shown in Fig. 2F, 0.4 μg protein was mixed in 2× sample buffer (62.5 mM Tris-HCl, pH 6.8, 40% glycerol, 0.01% bromophenol blue), left unboiled, and run in 25 mM Tris, pH 8.3, 0.192 M glycine.

Permeability assay. A total of 5×10^5 T84 cells were seeded in 12-mm transwell inserts (PET membrane with 0.4-μm pore size; Corning, NY) and cultured for >20 days until transepithelial resistance was stable. The culture medium was changed every 2 to 3 days. The cells were exposed to DSG2 ligands (20 μg/ml) in adhesion medium (DMEM, 1% FBS, 2 mM $MgCl_2$, 20 mM HEPES) for 15 min at room temperature. One mCi of [^{14}C]polyethylene glycol 4000 ([^{14}C]PEG-4000) (Perkin Elmer, Covina CA) diluted with DMEM-K12 medium was added to the inner chamber. Medium aliquots were harvested from the inner and outer chambers at 15 and 30 min and measured by a scintillation counter. Permeability was calculated as described elsewhere (36).

Trastuzumab cytotoxicity assay. For the trastuzumab cytotoxicity assay, 5×10^4 BT474-M1 cells/well were plated in triplicate in 96-well plates and grown to confluence. Ad3 fiber knobs or monoclonal antibodies (5 μg/ml) were added to the inner chamber. One hour later, trastuzumab (Genentech, San Francisco, CA) (15 μg/ml) was added, and cell viability was measured 2 h later by WST-1 assay (Roche, San Francisco, CA). Three independent studies were performed.

Immunofluorescence analyses. Cells were cultured in eight-chamber glass slides (BD Falcon), washed twice with ice-cold PBS, and then fixed with methanol-acetone (1:1, vol/vol) for 15 min at 4°C or with 4% paraformaldehyde for 30 min at 4°C. After fixation, cells were washed with PBS twice and blocked with 500 μl PBS–2% dry-milk powder for 20 min at room temperature. Antibody staining was performed in 100 μl PBS for 90 min at 37 or 4°C overnight. If needed, secondary antibodies directed against the appropriate host were added after three washes with PBS for 45 min at room temperature. After three washes with PBS, glass slides were mounted using Vectashield with 4′,6′-diamidino-2-phenylindole (DAPI) (Vector Labs). Photographs were taken with a Leica DFC300FX digital camera. Confocal images were taken on a Zeiss META confocal microscope using 40× or 100× oil lenses and Zeiss 510 software (Zeiss MicroImaging, Thornwood, NY).

Electron microscopy (EM). Polarized cells in Transwell chambers were fixed with half-strength Karnovsky's fixative (2% paraformaldehyde, 2.5% glutaraldehyde, 0.2 M cacodylate buffer) for 1 h at room temperature. The fixative in the inner chamber contained 0.2% ruthenium red. The ruthenium red [ruthenium-(III) chloride oxide, ammoniated] was purchased from Alfa Aesar (Ward Hill, MA). Postfixation was performed with 1% OsO_4-phosphate buffer. The membranes were cut out from the Transwell chambers and embedded in Medcast (Ted Pella, Redding, CA). Ultrathin sections were stained with uranyl acetate and lead citrate. Processed grids were evaluated with a JEOL JEM1200EXII transmission electron microscope. Images were acquired with an Olympus SIS Morada digital charge-coupled-device camera using iTEM software for image processing.

siRNA studies. A set of DSG2 specific short interfering RNAs (siRNAs) was synthesized by Dharmacon (Thermo Scientific). The target sequences were CA AUAUACCUGUAGUAGAA, GAGAGGAUCUGUCCAAGAA, CCUUAG AGCUACGCAUUAA, and CCAGUGUUCUACCUAAAUA. Control siRNA was purchased from Qiagen, Valencia, CA. siRNA transfection was performed using HyperFect transfection reagent (Qiagen). A total of 1×10^5 HeLa cells were transfected with 1 μg DSG2 siRNA or control siRNA. Forty-eight hours after siRNA transfection, cells were collected with EDTA, and the attachment of ^{3}H-Ad3 or ^{3}H-Ad35 virus was analyzed as described above. Forty-eight h after siRNA transfection, cells were infected with Ad vectors at an MOI of 50 PFU/cells, and GFP expression was analyzed 18 h later.

SPR. For surface plasmon resonance (SPR) analyses, acquisitions were done on a BIAcore X instrument. HBS-N (GE Healthcare, Pittsburgh, PA) supplemented with 2 mM $CaCl_2$ was used as a running buffer in all experiments at a flow rate of 5 μl/min. Immobilization on a CM4 sensorchip (BIAcore) was performed using DSG2 (Leinco Technology, Inc.) at 0.1 μg/ml diluted in 10 mM sodium acetate buffer, pH 4.2, and injected for 10 min on an ethyl(dimethylaminopropyl) carbodiimide–*N*-hydroxysuccinimide (EDC-NHS)-activated flow cell. A control flow cell was activated by EDC-NHS and inactivated by ethanolamine. Different concentrations of Ad3 fiber knobs or PtDds were injected for a 5-min association followed by a 3-min dissociation, and the signal was automatically subtracted from the background of the ethanolamine-deactivated EDC-NHS flow cell.

For experiments using biotinylated ligands, two flow cells of a CM4 sensorchip were activated as described above and then coated by the injection of streptavidin (0.1 μg/ml in acetate buffer pH 4.1) for 5 min. Biotinylated ligands then were injected at 0.1 μg/ml in running buffer for 5 min on one of these two flow cells, the other being used for background subtraction during the run. Different concentrations of soluble DSG2 were injected in running buffer on these flow cells, and background was automatically subtracted.

Negative-stain electron microscopy. Recombinant fiber knob proteins were visualized by negative-stain EM to assess their assembly status. The standard mica-carbon preparation was used with protein at 0.1 mg/ml. Samples were stained using 1% (wt/vol) sodium silicotungstate (pH 7.0) and visualized on a Philips CM12 electron microscope at 100 kV.

Statistical analysis. All results are expressed as means ± standard deviations (SD). The Wilcoxon signed rank test was used when applicable. $P < 0.05$ was considered significant.

RESULTS

Chimeric Ad5 vectors containing Ad3 fibers use DSG2 as a receptor. Our preliminary studies indicated that the DSG2 interacting domain(s) within Ad3 is formed by the fiber or fiber/penton only in the spatial constellation that is present in viral particles, i.e., Ad3 virions or PtDds (33). To assess a potential role of Ad3 penton (which is present in PtDds) in binding to DSG2, we generated an Ad vector that contained Ad3 fibers (Ad5/3S-GFP) but that had all other capsid proteins (including the penton) derived from Ad5. To evaluate whether the Ad3 fiber shaft had a crucial role in Ad3-DSG2 interaction, e.g., contained DSG2 additional binding sites, we also generated a chimeric Ad5/3 vector that had the Ad3 shaft replaced by the Ad5 shaft (designated Ad5/3L-GFP) (Fig. 1A). Notably, while the Ad3 fiber shaft contains 6 shaft repeat motifs, the Ad5 shaft is longer and contains 22 shaft motifs. For comparison, we used an Ad3 vector (Ad3-GFP) containing the same GFP expression cassette as that of the Ad5/3 vectors (33). We analyzed whether Ad5/3S-GFP and Ad5/3L-GFP vectors use DSG2 for infection. The attachment of ^{3}H-labeled Ad vectors to HeLa cells was blocked by recombinant DSG2 protein to the same degree for Ad3-GFP, Ad5/3S-GFP, and Ad3/5L-GFP (Fig. 1B). As expected, recombinant DSG2 also blocked the transduction of all three vectors as measured based on GFP intensity 18 h after the infection of HeLa cells (Fig. 1C). PtDd,

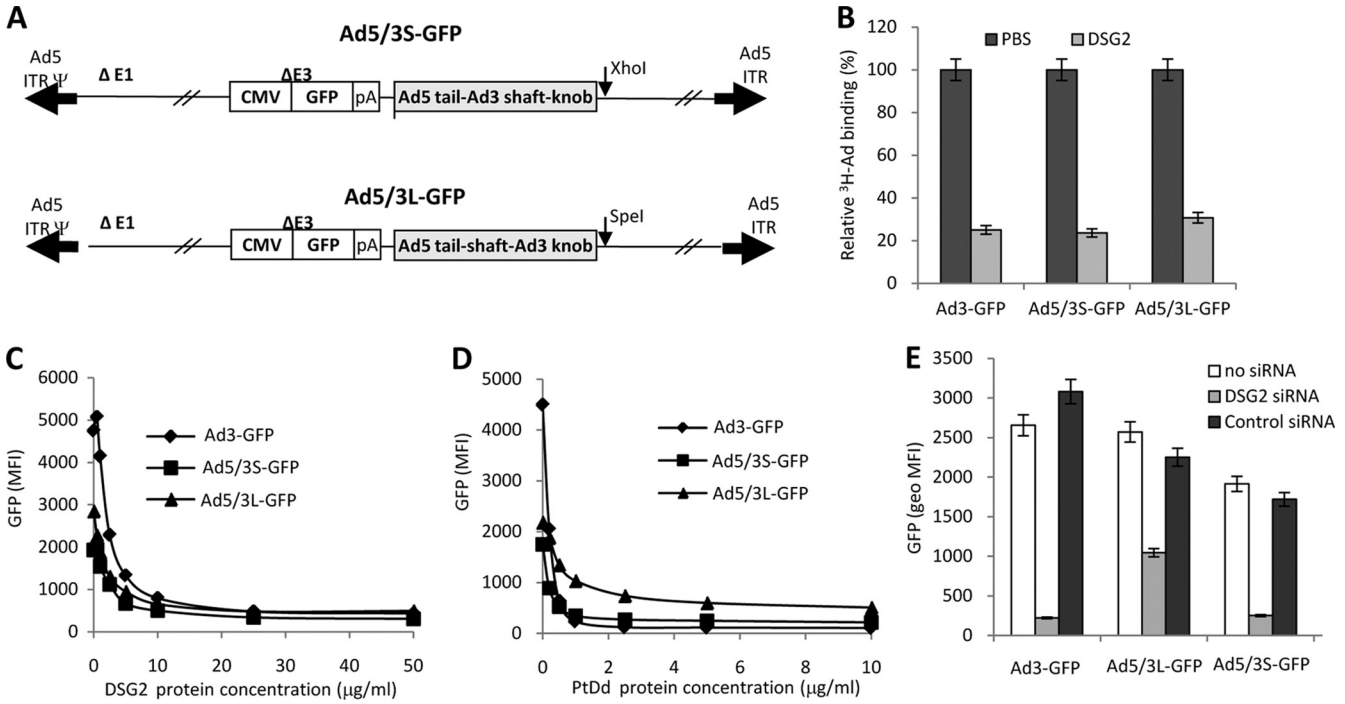

FIG. 1. Role of DSG2 in transduction of chimeric Ad5/3 vectors. (A) Structure of Ad5/3 vectors. The vectors are based on Ad5 and are deleted for the E1 and E3 regions. Both vectors contain a GFP expression cassette inserted into the E3 region. In Ad5/3L-GFP, the Ad5 fiber knob domain is replaced by that from Ad3. In Ad5/3S-GFP the Ad5 shaft and knob domains were replaced by the corresponding domains from Ad3. The Ad3 shaft domain contains 6 shaft motifs, while the Ad5 shaft domain contains 22 shaft motifs. ITR, inverted terminal repeat; pA, polyadenylation signal. (B) Blocking of Ad attachment by recombinant DSG2 protein. H^3-labeled Ads were incubated with 6 μg/ml of recombinant human DSG2 protein on ice for 1 h and then added to HeLa cells for 1 h on ice. Ad attachment to cells incubated with PBS instead of DSG2 was taken as 100%. $n = 3$, i.e., three separate wells. Ad3-GFP is a vector derived from Ad3 that contains the same GFP expression cassette as that of the Ad5/3 vectors. (C) Blocking of Ad transduction by recombinant DSG2 protein. Ad vectors were incubated with increasing concentrations of DSG2 protein at room temperature for 60 min. HeLa cells then were infected at an MOI of 100 PFU/cell for 60 min, after which the viruses were removed and new medium was added. GFP fluorescence was measured 18 h later by flow cytometry. $n = 3$. Shown are average values. The SD were less than 10% for all samples. (D) Competition of Ad infection by Ad3 PtDd. HeLa cells were incubated with increasing concentrations of PtDd for 60 min and then infected with Ad vectors at an MOI of 100 PFU/cell for 60 min, after which the viruses were removed and new medium added. GFP fluorescence was measured 18 h later. $n = 3$. Shown are average values. The SD were less than 10% for all samples. (E) DSG2 siRNA blocks infection of Ad5/3 vectors. A total of one microgram of siRNA was transfected onto 1×10^5 HeLa cells. Cells were collected 48 h after transfection by EDTA, and 1×10^5 cells were replated. On the second day, cells were infected with Ad vectors at an MOI of 100 PFU/cell. GFP fluorescence was measured 18 h later. geo MFI, geometric mean fluorescence intensity.

used as a competitor for DSG2 interaction domains within the Ad virions, blocked Ad3-GFP, Ad5/3S-GFP, and Ad3/5L-GFP transduction to similar levels (Fig. 1D). To prove the crucial role of DSG2 in the infection of Ad3 and Ad5/3 vectors, we transfected HeLa cells with siRNA specific to DSG2 mRNA or control siRNA. The mean fluorescence DSG2 intensity at 48 h after the transfection of siRNA was 22.1 and 195 for DSG2 siRNA- and control siRNA-transfected HeLa cells, respectively, indicating the efficient inhibition of DSG2 expression by DSG2 siRNA. DSG2 mRNA knockdown significantly decreased Ad3-GFP, Ad5/3S-GFP, and Ad3/5L-GFP transduction ($P < 0.001$) (Fig. 1E). Interestingly, the knockdown of DSG2 decreased Ad5/3L-GFP transduction to a lesser degree ($P < 0.01$) than the transduction of the vectors containing Ad3 fibers (Ad3-GFP and Ad5/3S-GFP). We speculate that Ad5/3L-GFP can use receptors other than DSG2. Taken together, these studies show that Ad5/3 vectors use DSG2 as a receptor. This has relevance for clinical studies because Ad5/3 vectors are used in patients (14, 35). In addition, the DSG2-interacting domains of Ad3 are located within the fiber. It appears that the Ad pentons (within PtDds or Ad5 and Ad3 virions) merely provide a scaffold for the correct spatial constellation of Ad3 fiber knobs for interaction with DSG2.

Cross-linking of Ad3 fiber knobs is required for efficient binding to DSG2. We then focused our attention on the Ad3 fiber. We produced in *E. coli* a series of recombinant Ad3 fiber knob proteins containing the fiber knob and increasing numbers of Ad3 shaft repeats (from one to six repeats) (Fig. 2A). Western blot analyses using DSG2 or anti-Ad3 fiber knob antibodies showed that all recombinant fiber knobs formed trimers (Fig. 2B and C). As observed previously (33), the Ad3 fiber knob plus one shaft domain (S/Kn) did not bind DSG2 in Western blot analyses, indicating a potential steric influence of the shaft motif on the Ad3 knob conformation. The protein containing six shaft motifs (S6/Kn) tended to form aggregates and was not used in further studies. When used in competition studies, all recombinant fiber knob proteins inhibited Ad3-GFP transduction significantly less than PtDds (Fig. 2D and E). We then attempted to test whether Ad3 fiber knob dimerization would increase DSG2 binding. Because all re-

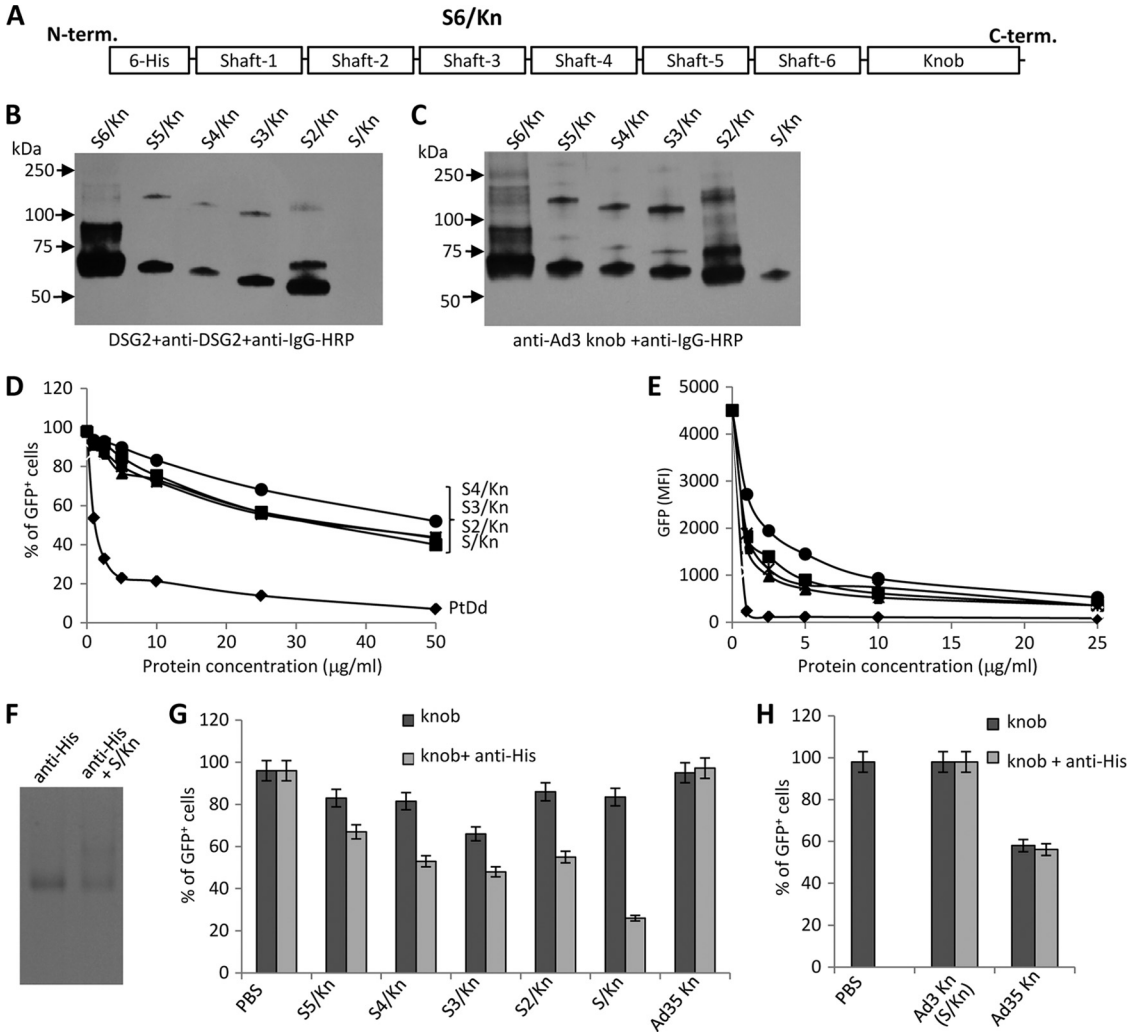

FIG. 2. Blocking of Ad3 infection requires cross-linking of Ad3 fiber knobs. (A) Structure of a recombinant Ad3 fiber knob (S6/Kn) containing an N-terminal His tag, six shaft motifs (S6), and the knob domain (Kn). Additional fiber knob variants contained 5, 4, 3, 2, or 1 shaft motif and were labeled S5/Kn, S4/Kn, S3/Kn, S2/Kn, and S/Kn, respectively. (B) Western blot analysis of recombinant Ad3 fiber knobs. Filters were incubated with recombinant DSG2, followed by mouse monoclonal anti-DSG2 antibodies and anti-mouse IgG horseradish peroxidase conjugates. Visible are trimeric forms of the Ad3 fiber knobs in the range of 50 to 70 kDa. The theoretical molecular masses of (trimeric) S6/Kn, S5/Kn, S4/Kn, S3/Kn, S2/Kn, and S/Kn are 93.9, 89.7, 84.3, 79.2, 74.4, and 69.3 kDa. S6/Kn and S2/Kn formed more multimers of fiber knobs (>75 kDa) than the other knobs and tended to generate inclusion bodies in *E. coli*. The denaturation of fiber knobs would result in 25- to 30-kDa monomers (not shown). (C) Western blot using antibodies against the Ad3 fiber knob as a probe. (D and E) Competition of Ad3-GFP transduction. HeLa cells were incubated with increasing concentrations of PtDd and different Ad3 fiber knobs for 60 min and then infected with Ad3-GFP at an MOI of 100 PFU/cell for 60 min, after which the viruses were removed and new medium added. GFP fluorescence was measured 18 h later. $n = 3$. Shown are average values of percent GFP-positive cells (D) and mean GFP fluorescence (E). The SD were less than 10% for all samples. S5/Kn is not shown for clarity. (F) Cross-linking of the His-tagged fiber knob (S/Kn) by anti-His antibodies. Anti-His MAb was incubated with PBS or S/Kn for 60 min and run on a native polyacrylamide gel. The antibody has a molecular mass of 150 kDa. An additional band with a higher molecular mass appeared in the presence of S/Kn, reflecting a complex of both proteins. The knob alone is not shown. (G) Effect of the cross-linking of Ad3 fiber knobs with anti-His antibodies on the inhibition of Ad3-GFP transduction. Five μg/ml of Ad3 fiber knobs was incubated with 20 μg/ml of mouse anti-His MAb at room temperature for 60 min and then added onto 1×10^5 HeLa cells. After 60 min of incubation, 100 PFU/cell of Ad3-GFP virus was added and GFP was analyzed as described for panel D. The differences between knob and knob plus anti-His were significant ($P < 0.005$) for all Ad3 fiber knobs. For comparison, we also included an Ad35 fiber knob (nondimerizing) in this study. (H) Effect of cross-linked Ad3 or Ad35 fiber knobs on Ad35-GFP transduction. Ad35-GFP is a vector derived from Ad35 containing a CMV-GFP expression cassette (33). Ad3 and Ad35 fiber knobs are proteins that contain a His tag, one shaft motif, and the corresponding knobs (31). (The Ad3 knob is the same as S/Kn). The experiment was performed as described for panel G. The difference between knob and knob plus anti-His was not significant.

combinant fiber knobs contained an N-terminal His tag (used for protein purification), we mixed Ad3 fiber knobs with antibodies against the His tag to achieve their cross-linking. The formation of complexes between anti-His tag antibodies and the fiber knob was demonstrated by electrophoresis in native polyacrylamide gels (Fig. 2F). When anti-His antibodies cross-linked fiber knobs were used as competitors, a significant inhibition of Ad3-GFP transduction (compared to fiber knobs mixed with control IgG) was observed (Fig. 2G), suggesting that dimers of Ad3 fiber knobs are required for DSG2 binding.

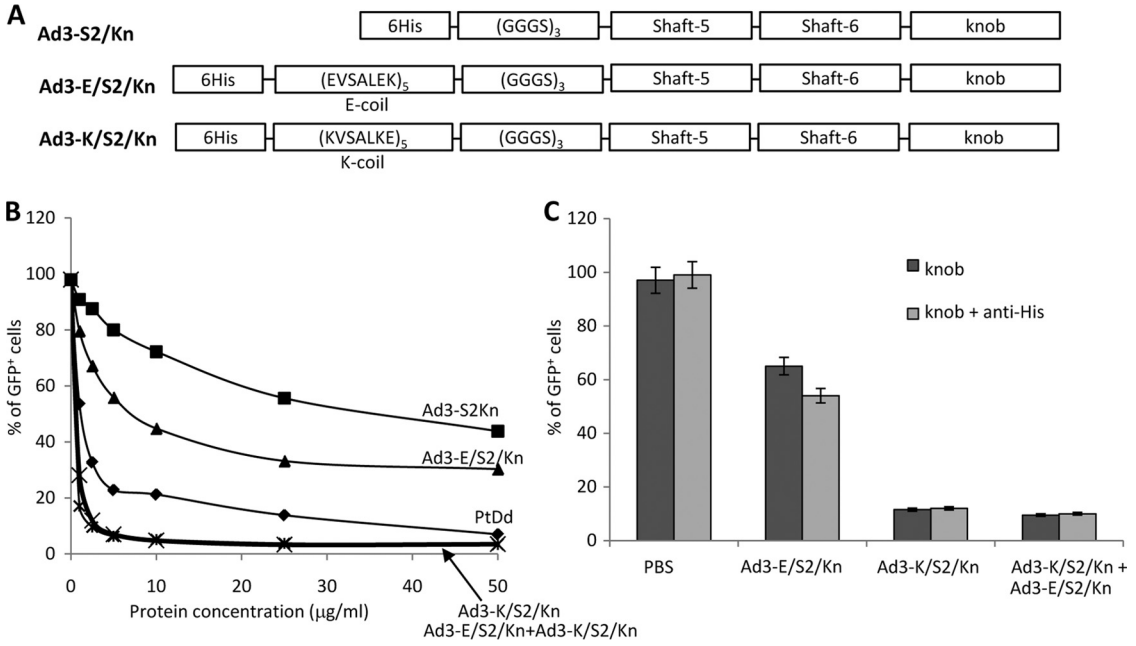

FIG. 3. Ad3 fiber knob dimerization via E/K coils. (A) Schematic structure of recombinant Ad3 fiber knob proteins containing an N-terminal His tag, dimerization domains (E coil or K coil [17]), a flexible linker, two fiber shaft motifs (fifth and sixth), and the Ad3 fiber knob domain. Ad3-S2/Kn is a fiber that lacks the dimerization domains. (B) Competition of Ad3-GFP transduction. HeLa cells were incubated with increasing concentrations of PtDd and different Ad3 fiber knobs for 60 min and then infected with Ad3-GFP at an MOI of 100 PFU/cell for 60 min, after which the viruses were removed and new medium added. GFP fluorescence was measured 18 h later. $n = 3$. Shown are average values of percent GFP-positive cells. Ad3-K/S2/Kn+Ad3-E/S2/Kn is a 1:1 mixture of both fiber knobs. PtDd versus Ad3-E/S2/Kn, $P = 0.074$; PtDd versus Ad3-K/S2/Kn + Ad3-E/S2/Kn, $P = 0.03$; Ad3-K/S2/Kn versus Ad3-K/S2/Kn + Ad3-E/S2/Kn, $P = 0.62$. (C) Cross-linking of Ad3 fiber knobs with anti-His antibodies. Five μg/ml of Ad3 fiber knobs was incubated with 20 μg/ml of mouse anti-His MAb at room temperature for 60 min and then added to 1×10^5 HeLa cells. After 60 min of incubation, 100 PFU/cell of Ad3-GFP virus was added and GFP was analyzed as described for panel B. The difference between knob and knob plus anti-His is significant for Ad3-E/S2/Kn ($P < 0.05$) but not for the other samples.

This appeared to be a new Ad binding strategy unique to Ad3, because anti-His antibody cross-linking of the Ad35 fiber knobs had no effect on infection by the CD46-interacting vector Ad35-GFP (Fig. 2H).

Ad3 fiber knob dimers block Ad3 infection. Cross-linking with antibodies enhanced the blocking effect of Ad3 fiber knobs containing fewer shaft motifs than the wild-type Ad3 fiber knob. For a potential biotechnological application of Ad3 fiber knobs as junction openers, we focused our further studies on fiber knob variants with the minimum number of shaft motifs, i.e., S2/Kn. Based on the finding that fiber knob cross-linking increased binding to DSG2, we generated dimers of S2/Kn by incorporating dimerization domains. To avoid the spontaneous fiber knob dimerization and potential formation of inclusion bodies during production in *E. coli*, we utilized a heterodimeric system consisting of E-coil and K-coil peptides, which interact with each other with high affinity (17). Two fiber knob variants containing five repeats of EVSALEK (K-coil) and KVSALKE (E-coil), a G/S-rich flexibility domain followed by two shaft motifs, and the homotrimeric fiber knob domain were generated (Fig. 3A). Ad3-K/S2/Kn and Ad3-E/S2/Kn were produced separately in *E. coli* and purified by affinity chromatography. For dimerization, both purified proteins were mixed at a 1:1 concentration ratio. The mixture of Ad3-K/S2/Kn and Ad3-E/S2/Kn (designated Ad3-K/S2/Kn+Ad3-E/S2/Kn) blocked Ad3 infection as efficiently as PtDd (Fig. 3B). Interestingly, Ad3-K/S2/Kn alone had the same competing strength as the mixture of both peptides, while Ad3-E/S2/Kn alone only inefficiently blocked infection. This suggests that Ad3-K/S2/Kn is able to homodimerize while Ad3-E/S2/Kn is not. In support of this, we found that further cross-linking with anti-His antibodies increased the blocking effect of Ad3-E/S2/Kn ($P < 0.05$) but not that of Ad3-K/S2/Kn (Fig. 3C).

Binding of a minimal dimeric Ad3 fiber knob protein to DSG2. We then attempted to produce the smallest Ad3 fiber knob dimer, containing the K-coil or E-coil dimerization domain, only one shaft motif, and the homotrimeric Ad3 fiber knob (Ad3-K/S/Kn and Ad3-E/S/Kn) (Fig. 4A). Because of their smaller size, such proteins have potential advantages in egress from blood vessel and tissue penetration, and theoretically they also contain fewer immunogenic epitopes. Ad3-K/S/Kn and Ad3-E/S/Kn were produced in *E. coli* and purified by affinity chromatography. Analysis by polyacrylamide gel electrophoresis showed that the vast majority of Ad3-K/S/Kn and Ad3-E/S/Kn were present as trimers (~65 to 70 kDa) (Fig. 4B). Ad3-K/S/Kn alone and in combination with Ad3-E/S/Kn were analyzed by negative-stain electron microscopy to assess their assembly status (Fig. 4C). Dimers of fiber knobs and aggregates thereof were found for both Ad3-K/S/Kn and Ad3-K/S/Kn+Ad3-E/S/Kn, but larger aggregates were less abundant in Ad3-K/S/Kn preparations. Both Ad3-K/S/Kn and Ad3-K/S/Kn+Ad3-E/S/Kn blocked Ad3 attachment to HeLa cells at a level comparable to that of PtDds (Fig. 4D). The preincubation of HeLa cells with Ad3-K/S/Kn and Ad3-K/S/

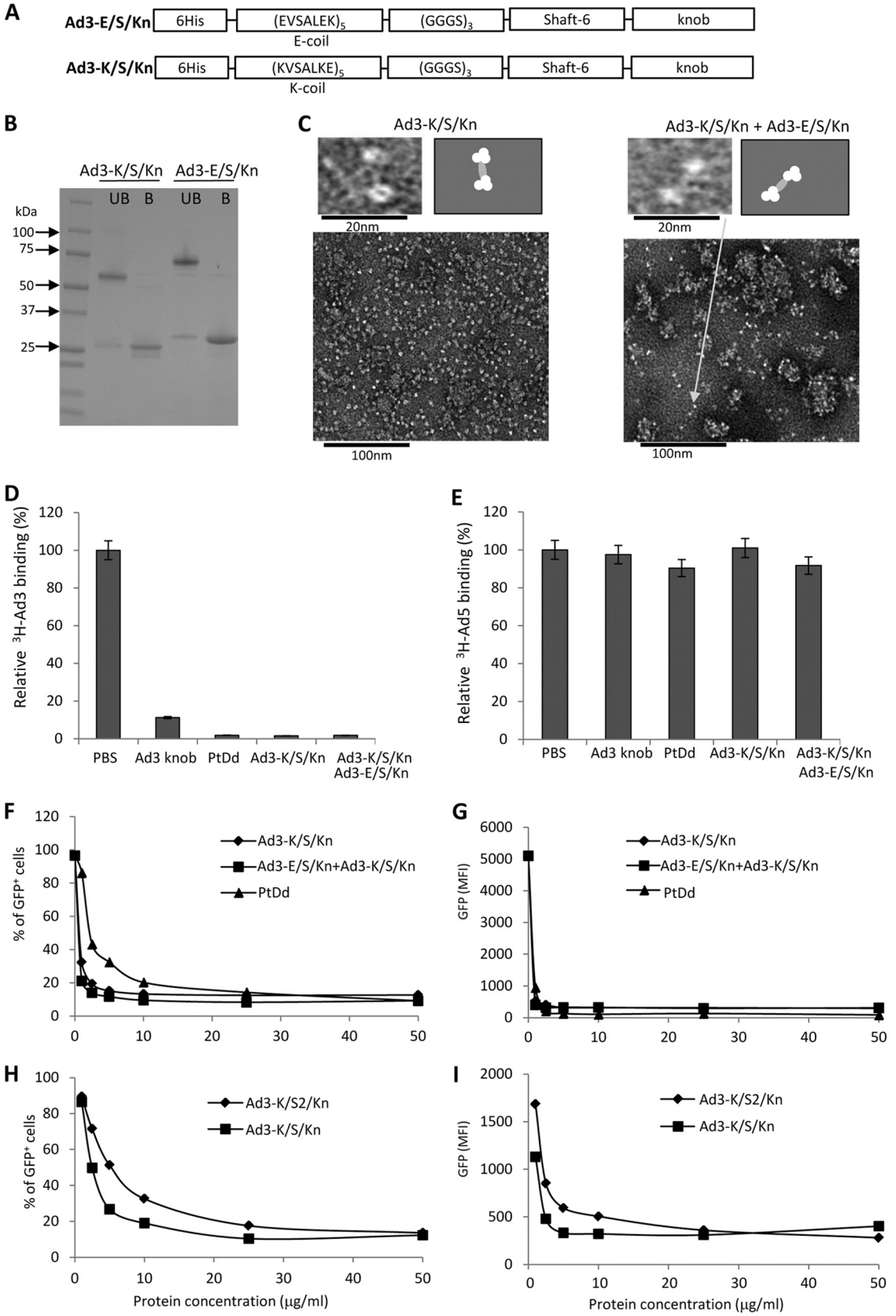

FIG. 4. Analysis of dimeric fiber knobs containing only one shaft motif. (A) Schematic structure of recombinant Ad3 fiber knob proteins Ad3-K/S/Kn and Ad3-E/S/Kn. The theoretical molecular mass of each fiber knob trimer is ~60 kDa. (B) Coomassie blue-stained gel. Samples were run on a 4 to 15% gradient polyacrylamide gel in Tris–glycine–0.1% SDS buffer. UB, unboiled samples; B, boiled samples. Note that boiling in

Kn+Ad3-E/S/Kn did not affect Ad5 attachment (Fig. 4E). As expected, Ad3-K/S/Kn and Ad3-K/S/Kn+Ad3-E/S/Kn also efficiently inhibited Ad3 infection (Fig. 4F and G). A side-by-side comparison of the fiber knobs with two and one shaft motif did not reveal significant differences in their ability to block Ad3 infection (Fig. 4H and I).

SPR analysis of dimeric Ad3 fiber knob binding to DSG2. To study the interaction of Ad3-K/S/Kn and Ad3-K/S/Kn+Ad3-E/S/Kn with DSG2 in more detail, we performed surface plasmon resonance (SPR) studies. We initially designed binding experiments in which DSG2 molecules were allowed to bind to immobilized fiber knobs (Fig. 5A). For immobilization, fiber knobs were biotinylated and linked via streptavidin to sensorchips. Kinetics analyses showed that both Ad3-K/S/Kn and Ad3-K/S/Kn+Ad3-E/S/Kn similarly recognized DSG2 with a low dissociation at the end of injection. Clearly, the binding of soluble DSG2 to fibers only poorly mimics the physiological interaction between a cell surface and the virus. We therefore immobilized the receptor, DSG2, at the sensorchip surface and injected Ad3-K/S/Kn and Ad3-K/S/Kn+Ad3-E/S/Kn, and, for comparison, PtDd and (monomeric) Ad3 fiber knob at concentrations that give similar SPR responses (Fig. 5B). The outcome of these studies should depend on the valence of the fiber knobs, which is trimeric for Ad3 fiber knob (monomer), 2× trimeric for Ad3-K/S/Kn and Ad3-K/S/Kn+Ad3-E/S/Kn, and 12× trimeric for PtDds. It is further complicated by the fact that within the PtDd not all fibers can simultaneously interact with DSG2. While the association of the fiber knob dimers was similar (Fig. 5C), there were clear differences in the dissociation behavior. Ad3 fiber knob (nondimerizing; described previously [33]) dissociated faster than the other three ligands. Almost no dissociation was seen for PtDd and Ad3-K/S/Kn+Ad3-E/S/Kn. Ad3-K/S/Kn dissociation was between that of the Ad3 fiber knob and Ad3-K/S/Kn+Ad3-E/S/Kn. Although complex, these data clearly show that dimeric Ad3-K/S/Kn and Ad3-K/S/Kn+Ad3-E/S/Kn dissociate slower from DSG2 than does the Ad3 fiber knob. This can be explained by an avidity mechanism, implying that Ad3-K/S/Kn and Ad3-K/S/Kn+Ad3-E/S/Kn bind to several DSG2 molecules; a mechanism that allows the achieving of an overall low dissociation rate and highly stable attachment. Notably, although it is possible that all dimers in Ad3-K/S/Kn+Ad3-E/S/Kn are formed by Ad3-K/S/Kn, differences in dissociation rates argue against it. Further studies are required to prove this in detail.

The interaction of Ad3 with several DSG2 molecules is supported by immunofluorescence analyses of epithelial cells (Fig. 5D and E). These studies, using Cy3-labeled Ad3 virions, suggest that one virion clusters several DSG2 proteins around itself. As outlined later, we hypothesize that this specific clustering of receptors has functional consequences with regard to triggering intracellular signaling and opening epithelial junctions. Notably, previously we showed that PtDd binding to DSG2 triggers an epithelial-to-mesenchymal transition (EMT) in epithelial cells resulting in the transient opening of intercellular junctions (33).

Multimeric DSG2 ligands (Ad3 virions, PtDds, and Ad3-K/S/Kn) trigger opening of epithelial junctions. Epithelial cells maintain several intercellular junctions (tight junctions, adherens junctions, gap junctions, and desmosomes), a feature which is often conserved in epithelial cancers *in situ* and in cancer cell lines (29). Figures 6A shows confocal immunofluorescence microscopy images of polarized colon carcinoma T84 cells. Shown are the cells from the lateral side, i.e., stacked *x-z* layers. Intercellular junctions are visible as long vertical streaks marked by the adhesion junction protein claudin 7 and the desmosomal protein DSG2. DSG2 (green) is localized at the apical end of claudin 7 signals. The tight-junction protein ZO-1 can be found further apical of DSG2 (Fig. 6A, lower). The latter also is visualized in *x-y* images, which show a chicken-wire network of tight junctions marked by ZO-1 at the apical cell surface, whereas a section taken 1 μm deeper shows DSG2 staining (Fig. 6B). Importantly, the exposure of T84 cells to Ad3-K/S/Kn triggered the partial dissolution of epithelial junctions, which is reflected in decreased staining for DSG2 and ZO-1 (Fig. 6C) compared to that of untreated cells (Fig. 6A, lower).

The opening of epithelial junctions by Ad3-K/S/Kn was further confirmed by EM studies. EM images of untreated epithelial cells show intact tight and desmosomal junctions, as judged by the exclusion of the apically applied dye ruthenium red from basolateral space (Fig. 6D, left). The dye appears as an electron-dense line along the cell membrane surface. The incubation of epithelial cells with Ad3-K/S/Kn resulted in the leakage of ruthenium red deep into the lateral space within 1 h of Ad3-K/S/Kn addition (Fig. 6D, right). The partial disassembly of desmosomes (marked by arrows) in Ad3-K/S/Kn-treated cells is clearly visible in Fig. 6E. In addition to Ad3-K/S/Kn, the opening of epithelial junctions was observed in confocal immunofluorescence and EM studies with Ad3 virions, PtDd, and Ad3-K/S/Kn+Ad3-E/S/Kn (data not shown). The exposure of cells to the Ad3 fiber knob (nondimerizing) or Ad3-E/S/Kn, i.e., DSG2 ligands that are unable to multimerize, had no effect on epithelial junctions (data not shown). These studies indicate that the opening of epithelial junctions requires dimers or multimers of Ad3 fiber knobs.

Laemmli buffer disrupts the trimeric protein structures, resulting in ~25-kDa fiber knob monomers. (C) Negative-stain electron microscopy of purified Ad3-K/S/Kn and Ad3-K/S/Kn mixed with Ad3-E/S/Kn. The upper left image shows fiber knob dimers in both preparations. Note that the fiber knob itself is a trimer. The lower images show aggregates that contain more than two fiber knobs. The right panels show schematic drawings of the photographs. (D) Blocking of ^{3}H-Ad3 attachment by recombinant Ad3 fiber knobs or PtDd. Ad attachment to cells incubated with PBS was taken as 100%. $n = 3$. (E) Blocking of ^{3}H-Ad5 attachment by recombinant Ad3 fiber knobs or PtDd. Ad attachment to cells incubated with PBS was taken as 100%. $n = 3$. (F and G) Competition of Ad3-GFP transduction. HeLa cells were incubated with increasing concentrations of fiber knobs or PtDd for 60 min and then infected with Ad3-GFP at an MOI of 100 PFU/cell for 60 min, after which the viruses were removed and new medium added. GFP fluorescence was measured 18 h later. $n = 3$. Shown are average values of percent GFP-positive cells (F) and mean GFP fluorescence (G). The SD were less than 10% for all samples. (H and I) The same study as that described for panels F and G was performed but with Ad3-K/S/Kn and the fiber knobs with two shaft motifs, Ad3-K/S2/Kn.

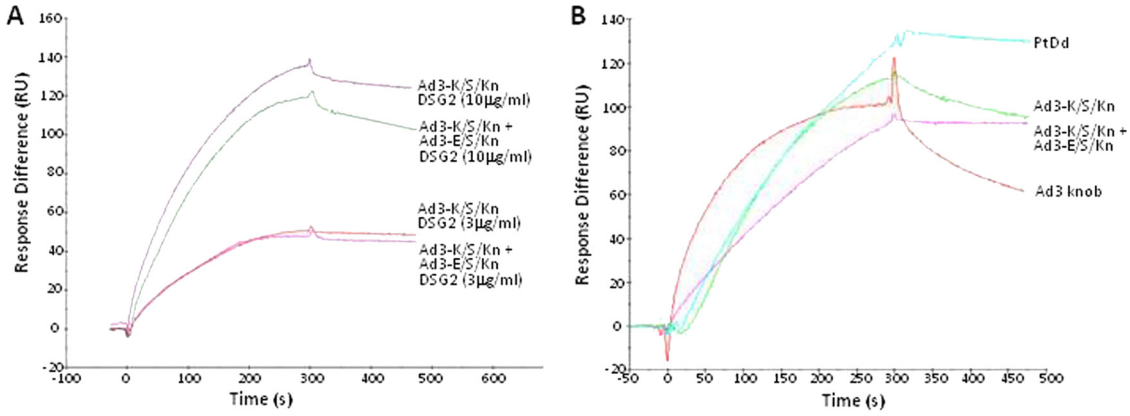

C

	Binding at the end of association	Remaining binding after 150s dissociation	% of remaining binding after 150s
AdB knob	101.4	64.1	63.2
AdB-K/S/Kn + AdB-E/S/Kn	93.7	92.6	98.8
AdB-K/S/Kn	112.8	96.9	85.9
PtDd	133.1	130.5	98.0

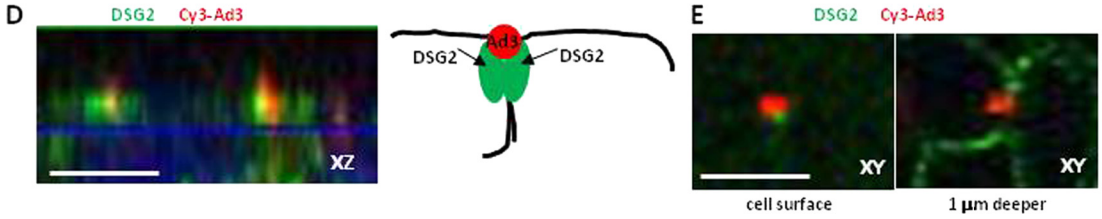

FIG. 5. SPR analysis of Ad3-K/S/Kn+Ad3-E/S/Kn and Ad3-K/S/Kn interaction with DSG2. (A) Biotinylated fiber knobs were immobilized to streptavidin-linked sensorchips. DSG2 was injected at 3 and 10 mg/ml. Response signals were collected during the indicated time periods with automatic background subtraction. RU, relative units. (B) DSG2 was immobilized on sensorchips, and background was automatically subtracted from the control flow cell. The injection of the Ad3 fiber knob (nondimerizing), Ad3-K/S/Kn, and Ad3-E/S/Kn+Ad3-K/S/Kn at 10 μg/ml and PtDd at 3 μg/ml to normalize all responses to about 100 RU (taking into account that a dodecahedron has 12 fibers and that the SPR signal depends on the molecular size of the analyte). (C) Summary of SPR data shown in panel B and calculation of remaining signal 150 s after the end of injection. (D) Confocal immunofluorescence analysis of DSG2 and Ad3 particles on epithelial colon cancer T84 cells. Shown are cells from the lateral side, i.e., stacked *x-z* confocal image layers. Cells were exposed to Cy3-labeled Ad3 particles for 15 min, washed, fixed, and stained with anti-DSG2 antibodies (green). Ad3 particles appear in red. The scale bar is 20 μm. The panel on the right shows a schematic drawing of the confocal image with two DSG2 units clustered by the Ad3 particle. (E) *x-y* sections of the cell surface and 1 μm deeper. The images suggest that Ad3 binds to DSG2 molecules that are exposed on the cells surface. Note that most of the DSG2 is localized and deeper, i.e., is distal of tight junctions.

In addition to leakage studies with ruthenium red, we used three functional assays to demonstrate the opening of epithelial junctions by Ad3-K/S/Kn. (i) Exposure of polarized epithelial cells to Ad3-K/S/Kn increased the transepithelial permeability within 30 min, as shown by [^{14}C]PEG-4000 transflux studies (Fig. 7A). Importantly, permeability after incubation with nondimerizing Ad3-E/S/Kn fiber knobs or monoclonal antibodies against different regions of the extracellular domain of DSG2 was >5-fold lower than that after incubation with Ad3-K/S/Kn. (ii) Previous studies showed that in polarized breast cancer BT474-M1 cells, Her2/*neu*, the target for herceptin/trastuzumab, is trapped in epithelial junctions, and that the incubation of BT474-M1 cells with Ad3 PtDd increases access to Her2/*neu* and increases the trastuzumab killing of cancer cells (33). Here, we used this assay to study the effect of additional DSG2 ligands on trastuzumab cytotoxicity (Fig. 7B). We found that Ad3-K/S/Kn significantly increased the killing of BT474-M1 cells by trastuzumab. In contrast, DSG2 ligands that are not able to dimerize, i.e., Ad3-E/S/Kn and a series of anti-DSG2 antibodies, had no significant effect on trastuzumab killing. Notably, one of the anti-DSG2 antibodies against extracellular domains 3 and 4 (MAb 6D8) appeared to stimulate tumor cell proliferation. (iii) CAR, the receptor for Ad5, is localized in tight junctions of polarized T84 epithelial cells (3). This is shown by confocal immunofluorescence microscopy of T84 cells (Fig. 7C, upper, and D, upper). The incubation of these cells with Ad3-K/S/Kn greatly increased CAR staining, which now appeared along the lateral membranes (Fig. 7C, lower) and at the cell surface (Fig. 7D, lower). We speculated that this is the result of the disassembly of tight junctions and

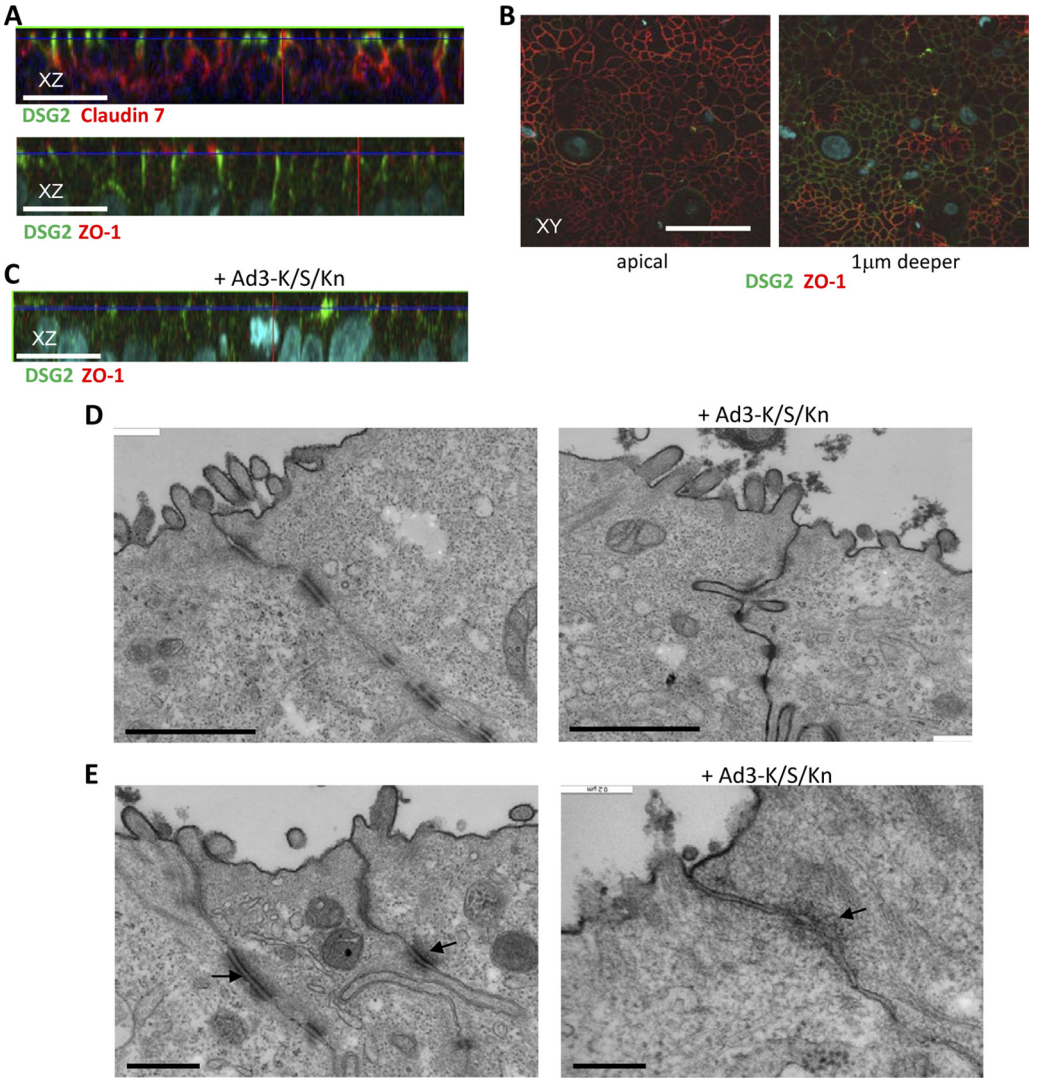

FIG. 6. Analysis of epithelial junctions. Studies were performed on polarized colon carcinoma T84 cells cultured for 20 days in transwell chambers. (A) Confocal immunofluorescence microscopy. Shown are representative stacked *x-z* images. In the upper panel, DSG2 (green) appears at the apical site of basolateral junctions marked by claudin 7 (red). In the lower panel, the tight junction marker ZO-1 (red) is localized at the apical side of DSG2 (green). Claudin 7 staining masks the lower part of DSG2 streaks in the lateral membrane, while ZO-1 staining covers the upper part of DSG2 signals. The scale bar is 20 μm. (B) Shown are *x-y* sections from the cell surface and from 1 μm deeper stained for DSG2 (green) and ZO-1 (red). (C) Cells were treated with Ad3-K/S/Kn (5 μg/ml) and analyzed 12 h later for DSG2 and ZO-1. (D) Transmission electron microscopy of junctional areas of T84 cells. Cells were treated with PBS (left) or Ad3-K/S/Kn (right) for 1 h on ice, washed, and then incubated for 1 h at 37°C. At this time, the electron-dense dye ruthenium red (1) was added together with the fixative. If tight junctions (above the desmosomes) are closed, the dye only stains the apical membrane (black line). If tight junctions are open, the dye penetrates between the cells and stains the basolateral membrane. The scale bar is 1 μm. Magnification is 40,000×. (E) A larger magnification (100,000×) shows the disintegration of desmosomes (marked by an arrow) after Ad3-K/S/Kn treatment. The scale bar is 0.2 μm.

the better accessibility of CAR to anti-CAR antibodies that were applied to the apical side of T84 cells. Another potential assay for the disruption of tight junctions and CAR accessibility is transduction with a CAR-targeting Ad vector. The infection of polarized T84 cells (apical side) with Ad5-GFP at an MOI of 250 PFU/cell resulted in the transduction of 8% ± 2% of cells (based on GFP-positive cells counted 20 h after infection) (Fig. 7E). Ad5-GFP infection in the presence of Ad3-K/S/Kn yielded 38% ± 9% of GFP-positive cells. Ad3-GFP in the presence of dilution buffer or Ad3-K/S/Kn transduced 17% ± 6% or 68% ± 17% of T84 cells, respectively. The latter is in agreement with an earlier study showing that Ad3 infects polarized epithelial cells more efficiently than Ad5 (28). This most likely is due to its ability to bind to DSG2 and trigger junction opening. Ad3-K/S/Kn increased Ad3-GFP transduction. We speculate that the relatively small Ad3-K/S/Kn protein and its high concentration initially reaches more DSG2 receptors than Ad3 virions and thus enhances the opening of tight junctions. In all settings shown in Fig. 7E, most cells at the periphery of the monolayers (i.e., cells that are in contact with the walls of the inner chamber, without tight junctions) were GFP positive. We therefore counted GFP-positive cells in

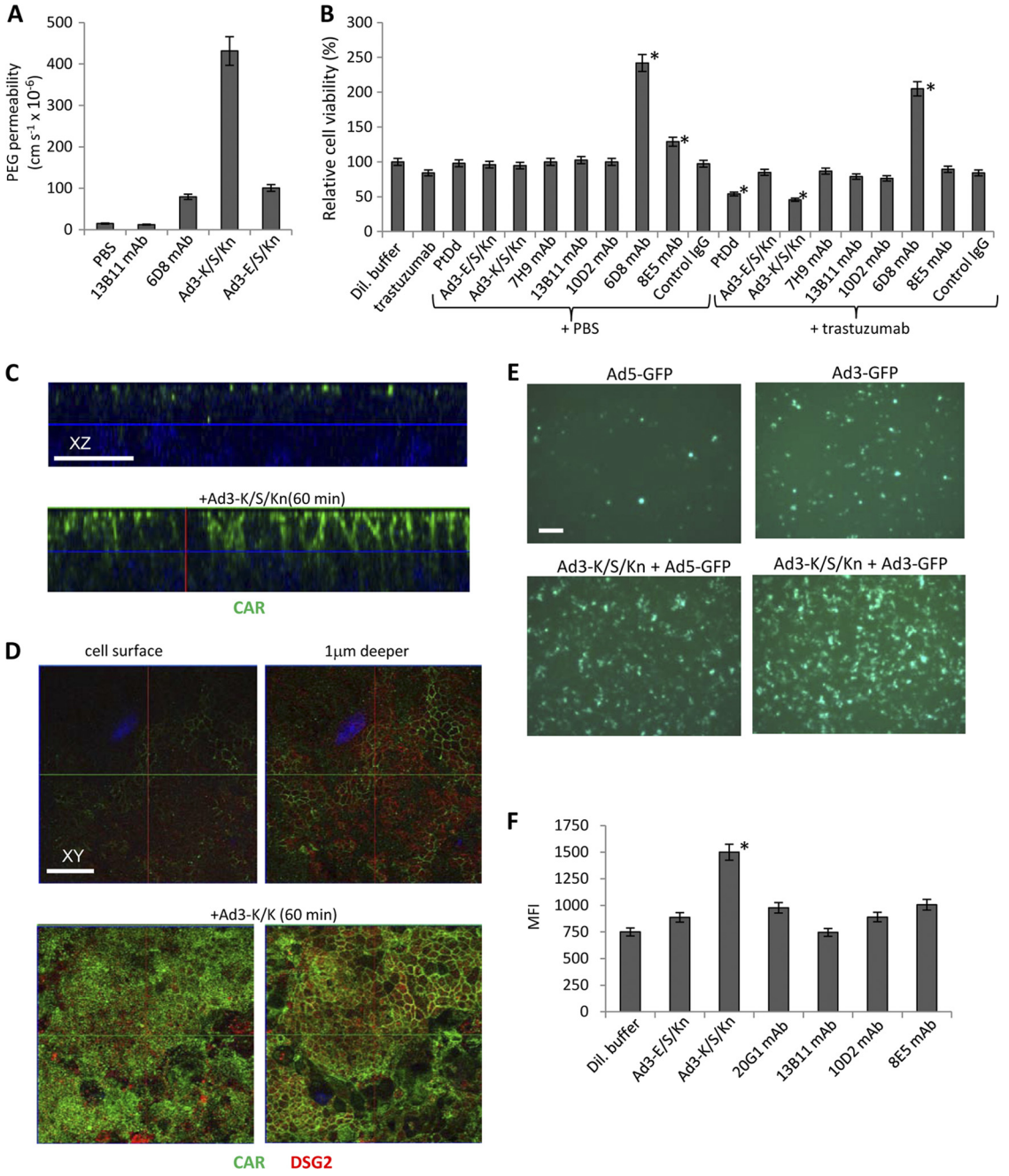

FIG. 7. Functional analyses of epithelial junction opening. (A) T84 cells were grown in polyester membrane transwell inserts for 21 days until transepithelial resistance was constant, implying that tight intercellular junctions had formed. Shown is [^{14}C]PEG-4000 diffusion through polarized T84 cells cultured in transwell chambers. Cells were incubated with PBS or the various DSG2 ligands for 15 min, after which [^{14}C]PEG-4000 was added to the inner chamber. Paracellular flux was assessed in aliquots from the apical and basal chambers as described elsewhere (1). The following monoclonal antibodies against different extracellular domains (ECD) of DSG2 were used: 13B11-MAb (against ECD 1 and 2) and 6D8-MAb (against ECD 3 and 4). Ad3-K/S/Kn is the dimerizing form. Ad3-E/S/Kn is unable to dimerize. (B) Effect of DSG2 ligands on trastuzumab killing of Her2/*neu*-positive breast cancer BT474-M1 cells. Cells were incubated at 100% confluence for 2 days. Ligands were added to the inner chamber for 1 h, followed by PBS or trastuzumab. Cell viability was measured 2 h later (see Materials and Methods). In addition to 13B11 and 6D8 MAbs, the following anti-DSG2 antibodies were used: 7H9 (against the propeptide domain), 10D2 (against ECD 2), and 8E5 (against ECD 3 and 4). The viability of dilution buffer-treated cells was taken as 100%. $n = 5$, i.e., five separate wells. $*$, $P < 0.05$ compared to data for dilution buffer. (C) Confocal microscopy for CAR in T84 cells treated with dilution buffer or Ad3-K/S/Kn (stacked *x-z* layers). T84 cells were grown in polyester membrane transwell inserts for 21 days. Ad3-K/S/Kn (40 μg/ml) or dilution buffers were added for 60 min, after which cells were washed and subjected to immunofluorescence analysis. CAR appears as green staining. Nuclei are blue. The scale bar is 20 μm. (D) Confocal microscopy for CAR in polarized T84 cells. *x-y* images were taken from the cell surface and at a layer 1 μm beneath the cell surface (right). Experimental conditions were the same as those for panel C. The scale bar is 20 μm. (E) Ad transduction of T84 cells. T84 cells were grown in polyester membrane transwell inserts for 21 days. Ad3-GFP and Ad5-GFP were added to the inner chamber at an MOI of 250 PFU/cell together with dilution buffer (upper) or Ad3-K/S/Kn (40 μg/ml). Three hours later, virus was removed and cells were washed. GFP expression was analyzed after 20 h of incubation. Shown are representative images. For quantification, GFP-positive cells from 10 independent images of three independent experiments were counted. The scale bar is 20 μm. (F) Flow cytometry of Ad5-GFP-infected cells. T84 cells were infected with Ad5-GFP as described for panel E either in dilution buffer or 40 μg/ml DSG2 ligands. $n = 3$. $*$, $P < 0.05$ compared to data for dilution buffer.

fields at the center of transwells. The latter has to be considered in the interpretation of the flow cytometry analysis of GFP expression after Ad5-GFP infection in the presence of dilution buffer or Ad3-K/S/Kn (Fig. 7F). Although background GFP fluorescence levels were relatively high, the presence of Ad3-K/S/Kn, but not the presence of Ad3-E/S/Kn or anti-DSG2 MAbs, significantly increased GFP expression levels after Ad5-GFP infection.

Overall, our functional studies showed that Ad3-K/S/Kn can trigger the opening of epithelial junctions, while ligands that are unable to multimerize had no effect on junctions.

DISCUSSION

In this study, we describe two findings: (i) the multimerization of the Ad3 fiber knob is required to achieve high-affinity and stable binding to DSG2, and (ii) the multimeric mode of Ad3 fiber knob-DSG2 interaction triggers the opening of epithelial junctions.

Most Ad infections, including infection by the CAR-interacting Ad5, the DSG2-interacting Ad3, and the CD46-interacting Ad35 (22), target the airway epithelium. Achieving high-avidity binding to receptors with a low dissociation rate appears to be crucial for Ad infection to maintain contact between virus and target cells and, more importantly, to trigger subsequent events that allow the virus to disrupt the epithelial barrier, enter the target cells, and spread within the target tissue. For CAR- and CD46-binding Ads, high-avidity binding is achieved through interaction between the trimeric fiber knob and three receptor units. Furthermore, as shown for the interaction between Ad11 and CD46, initial Ad binding to the receptor can trigger conformational changes in the receptor to stabilize the binding (21), although it remains to be shown that the latter mechanism is used by Ads other than Ad11. For CAR- and CD46-interacting Ads, attachment involves the fiber knob and the receptor, and it can be completely blocked by an excess of soluble fiber knob. This is not the case for the DSG2-binding Ad3. We have shown that the complete inhibition of Ad3 binding and infection requires the physical linkage and, most likely, a specific spatial constellation of at least two fiber knobs. This is achieved with Ad virions, Ad3 PtDds, or dimeric Ad3-K/S/Kn. These ligands appear to achieve simultaneous binding to several DSG2 molecules, which on the one hand provides high avidity and on the other hand is functionally relevant for the opening of epithelial junctions. We currently are conducting crystal structure and mutagenesis studies to further support our findings on Ad3-DSG2 interaction.

To initiate infection, many pathogens have evolved mechanisms to disrupt junctional integrity. *Vibrio cholera* strains produce Zona occludens toxin (Zot), which possesses the ability to reversibly alter intestinal epithelial junctions, allowing the passage of macromolecules through mucosal barriers (6). *Clostridium perfringens* enterotoxin removes claudins 3 and 4 from the tight junctions to facilitate bacterial invasion (25). Furthermore, oncoproteins encoded by human Ad, human papillomavirus (HPV), and human T-cell leukemia virus type 1 (HTLV-1) can transiently open epithelial junctions by mislocalizing the junction protein ZO-1 (15). The latter mechanisms, used by viruses, appear to play a role in lateral viral spread. However, for an efficient initial infection, the attachment of virus must be linked with triggering the opening of epithelial junctions.

Recently, using immunofluorescence, phosphatidylinositol 3-kinase (PI3K)/mitogen-activated protein kinase (MAPK) phosphorylation, an mRNA expression array, and metabolic pathway inhibition approaches, we reported that the binding of DSG2 by Ad3 virions and Ad3 PtDds triggers an epithelial-to-mesenchymal transition in epithelial cells, resulting in the transient opening of intercellular junctions (33). Intercellular junction opening mediated by the interaction of Ad3 particles or recombinant PtDds with DSG2 was further supported by increased epithelial cell permeability and access to receptors that are trapped in intercellular junctions (e.g., Her2/*neu*) (33). In the present study, we provide morphological (confocal immunofluorescence and EM) and functional (permeability, trastuzumab killing, and Ad5 infection) data showing that Ad3-K/S/Kn also triggers junction opening. Importantly, other DSG2 ligands that are not able to multimerize and cluster DSG2, such as monomeric Ad3-E/S/Kn or monoclonal antibodies against different regions of DSG2, were unable to efficiently open junctions. The question remains how Ad3 can pass the tight junctions that are located at the apical side of DSG2/desmosomes. We speculate that efficient infection occurs through a positive feed-forward mechanism, because the Ad-DSG2-mediated junction opening occurs within minutes, thereby exposing DSG2 trapped in junctions to viral particles that are present at the site of infection.

In the discussion of Ad3 infection mechanisms, it is also noteworthy that, during Ad3 replication, PtDds are formed at a massive excess of 5.5×10^6 PtDds per infectious virus (7). This suggests that PtDd formation is functionally important for Ad3, i.e., advantageous in the spread or persistence of Ad3. A similar mechanism appears to work in the infection of epithelial cells by Ad5. During the replication of Ad5, the excess production of fiber results in the disruption of epithelial junctions either by interfering with CAR dimerization or by triggering intracellular signaling that leads to the reorganization of intercellular junctions (4, 32). Recently, it has been suggested (based on *in vitro* studies) that CD46 is exposed apically on polarized epithelial respiratory cells and therefore is more likely to function as an Ad receptor for initial infection *in vivo* (9). We could not confirm this in human CD46 transgenic mice, where the CD46 expression pattern did not correlate with Ad transduction (19). Moreover, in polarized epithelial cancer cultures, we found CD46 trapped in intercellular junctions and not accessible to Ad35 applied to the cell surface (33). At this point, we believe that the question of how CD46-binding Ads disrupt the epithelial barrier remains to be answered.

The finding that Ad3-K/S/Kn triggers junction opening has practical implications, because intercellular junctions represent physical obstacles for the access and intratumoral dissemination of anticancer therapeutics (26, 27). An epithelial junction opener would be relevant for cancer therapies with monoclonal antibodies directed against tumor-associated antigens that are trapped in epithelial junctions (e.g., Her2/*neu* or EGFR1) (33). A junction opener might also improve the efficacy of adoptive T-cell therapy (5) or treatment with liposomal chemotherapy drugs (10). Finally, Ad3-K/S/Kn might increase that efficacy of the transduction of normal or malignant tissues

by Ad5-based gene therapy vectors. The biotechnolocal applicability of Ad3-K/S/Kn is further underscored by the ease of its production and purification and by the fact that it spontaneously homodimerizes.

In conclusion, our study sheds light on the mechanisms of Ad3 infection of epithelial cells. The finding that Ad3-K/S/Kn, a small recombinant protein, triggers the opening of epithelial junctions has implications for cancer therapy and drug delivery into epithelial tissues. mfi, term.,

ACKNOWLEDGMENTS

The work was supported by NIH grants R01 CA080192 and R01 HLA078836.

We thank Christine Moriscot and Guy Schoehn from the IBS/UVHCI platform of the Partnership for Structural Biology in Grenoble (PSB/IBS) for Ad particle electron microscopy.

REFERENCES

1. **Arnberg, N.** 2009. Adenovirus receptors: implications for tropism, treatment and targeting. Rev. Med. Virol. **19:**165–178.
2. **Chitaev, N. A., and S. M. Troyanovsky.** 1997. Direct Ca2+-dependent heterophilic interaction between desmosomal cadherins, desmoglein and desmocollin, contributes to cell-cell adhesion. J. Cell Biol. **138:**193–201.
3. **Coyne, C. B., and J. M. Bergelson.** 2005. CAR: a virus receptor within the tight junction. Adv. Drug Deliv. Rev. **57:**869–882.
4. **Coyne, C. B., L. Shen, J. R. Turner, and J. M. Bergelson.** 2007. Coxsackievirus entry across epithelial tight junctions requires occludin and the small GTPases Rab34 and Rab5. Cell Host Microbe **2:**181–192.
5. **Disis, M. L.** 2009. Enhancing cancer vaccine efficacy via modulation of the tumor microenvironment. Clin. Cancer Res. **15:**6476–6478.
6. **Fasano, A., et al.** 1991. Vibrio cholerae produces a second enterotoxin, which affects intestinal tight junctions. Proc. Natl. Acad. Sci. U. S. A. **88:**5242–5246.
7. **Fender, P., A. Boussaid, P. Mezin, and J. Chroboczek.** 2005. Synthesis, cellular localization, and quantification of penton-dodecahedron in serotype 3 adenovirus-infected cells. Virology **340:**167–173.
8. **Fender, P., R. W. Ruigrok, E. Gout, S. Buffet, and J. Chroboczek.** 1997. Adenovirus dodecahedron, a new vector for human gene transfer. Nat. Biotechnol. **15:**52–56.
9. **Granio, O., et al.** 2010. Adenovirus 5-fiber 35 chimeric vector mediates efficient apical correction of the cystic fibrosis transmembrane conductance regulator defect in cystic fibrosis primary airway epithelia. Hum. Gene Ther. **21:**251–269.
10. **Harper, B. W., et al.** 2010. Advances in platinum chemotherapeutics. Chemistry **16:**7064–7077.
11. **Kälin, S., et al.** 2010. Macropinocytotic uptake and infection of human epithelial cells with species B2 adenovirus type 35. J. Virol. **84:**5336–5350.
12. **Keim, S. A., K. R. Johnson, M. J. Wheelock, and J. K. Wahl, 3rd.** 2008. Generation and characterization of monoclonal antibodies against the proregion of human desmoglein-2. Hybridoma **27:**249–258.
13. **Kirby, I., et al.** 2000. Identification of contact residues and definition of the CAR-binding site of adenovirus type 5 fiber protein. J. Virol. **74:**2804–2813.
14. **Koski, A., et al.** 2010. Treatment of cancer patients with a serotype 5/3 chimeric oncolytic adenovirus expressing GMCSF. Mol. Ther. **18:**1874–1884.
15. **Latorre, I. J., et al.** 2005. Viral oncoprotein-induced mislocalization of select PDZ proteins disrupts tight junctions and causes polarity defects in epithelial cells. J. Cell Sci. **118:**4283–4293.
16. **Lee, C., et al.** 2008. Targeting YB-1 in HER-2 overexpressing breast cancer cells induces apoptosis via the mTOR/STAT3 pathway and suppresses tumor growth in mice. Cancer Res. **68:**8661–8666.
17. **Litowski, J. R., and R. S. Hodges.** 2002. Designing heterodimeric two-stranded alpha-helical coiled-coils. Effects of hydrophobicity and alpha-helical propensity on protein folding, stability, and specificity. J. Biol. Chem. **277:**37272–37279.
18. **Lortat-Jacob, H., E. Chouin, S. Cusack, and M. J. van Raaij.** 2001. Kinetic analysis of adenovirus fiber binding to its receptor reveals an avidity mechanism for trimeric receptor-ligand interactions. J. Biol. Chem. **276:**9009–9015.
19. **Ni, S., et al.** 2006. Evaluation of adenovirus vectors containing serotype 35 fibers for tumor targeting. Cancer Gene Ther. **13:**1072–1081.
20. **Norrby, E., B. Nyberg, P. Skaaret, and A. Lengyel.** 1967. Separation and characterization of soluble adenovirus type 9 components. J. Virol. **1:**1101–1108.
21. **Persson, B. D., et al.** 2007. Adenovirus type 11 binding alters the conformation of its receptor CD46. Nat. Struct. Mol. Biol. **14:**164–166.
22. **Sanchez, M. P., D. D. Erdman, T. J. Torok, C. J. Freeman, and B. T. Matyas.** 1997. Outbreak of adenovirus 35 pneumonia among adult residents and staff of a chronic care psychiatric facility. J. Infect. Dis. **176:**760–763.
23. **Shayakhmetov, D. M., and A. Lieber.** 2000. Dependence of adenovirus infectivity on length of the fiber shaft domain. J. Virol. **74:**10274–10286.
24. **Shayakhmetov, D. M., T. Papayannopoulou, G. Stamatoyannopoulos, and A. Lieber.** 2000. Efficient gene transfer into human CD34(+) cells by a retargeted adenovirus vector. J. Virol. **74:**2567–2583.
25. **Sonoda, N., et al.** 1999. Clostridium perfringens enterotoxin fragment removes specific claudins from tight junction strands: evidence for direct involvement of claudins in tight junction barrier. J. Cell Biol. **147:**195–204.
26. **Strauss, R., and A. Lieber.** 2009. Anatomical and physical barriers to tumor targeting with oncolytic adenoviruses in vivo. Curr. Opin. Mol. Ther. **11:**513–522.
27. **Strauss, R., et al.** 2009. Epithelial phenotype of ovarian cancer mediates resistance to oncolytic adenoviruses. Cancer Res. **15:**5115–5125.
28. **Strauss, R., et al.** 2009. Epithelial phenotype confers resistance of ovarian cancer cells to oncolytic adenoviruses. Cancer Res. **69:**5115–5125.
29. **Turley, E. A., M. Veiseh, D. C. Radisky, and M. J. Bissell.** 2008. Mechanisms of Dis.: epithelial-mesenchymal transition-does cellular plasticity fuel neoplastic progression? Nat. Clin. Pract Oncol. **5:**280–290.
30. **Tuve, S., et al.** 2008. Role of cellular heparan sulfate proteoglycans in infection of human adenovirus serotype 3 and 35. PLoS Pathog. **4:**e1000189.
31. **Tuve, S., et al.** 2006. A new group B adenovirus receptor is expressed at high levels on human stem and tumor cells. J. Virol. **80:**12109–12120.
32. **Walters, R. W., et al.** 2002. Adenovirus fiber disrupts CAR-mediated intercellular adhesion allowing virus escape. Cell **110:**789–799.
33. **Wang, H., et al.** 2011. Desmoglein 2 is a receptor for adenovirus serotypes 3, 7, 11 and 14. Nat. Med. **17:**96–104.
34. **Wang, H., et al.** 2007. Identification of CD46 binding sites within the adenovirus serotype 35 fiber knob. J. Virol. **81:**12785–12792.
35. **Yang, S. W., et al.** 2011. Conditionally replicating adenovirus expressing TIMP2 for ovarian cancer therapy. Clin. Cancer Res. **17:**538–549.
36. **Yang, Z., M. Horn, J. Wang, D. D. Shen, and R. J. Ho.** 2004. Development and characterization of a recombinant Madin-Darby canine kidney cell line that expresses rat multidrug resistance-associated protein 1 (rMRP1). AAPS J. **6:**77–85.